The local effect of magnetic impurities on superconductivity in Co_xNbSe_2 and Mn_xNbSe_2 single crystals

2010 J. Phys.: Condens. Matter 22 015501

(http://iopscience.iop.org/0953-8984/22/1/015501)

J. Phys.: Condens. Matter **22** (2010) 015501 (6pp) doi:10.1088/0953-8984/22/1/015501

The local effect of magnetic impurities on superconductivity in Co_xNbSe_2 and Mn_xNbSe_2 single crystals

M Iavarone[1], G Karapetrov[1], J Fedor[1,3], D Rosenmann[1,4], T Nishizaki[2] and N Kobayashi[2]

[1] Materials Science Division, Argonne National Laboratory, Argonne, IL 60439, USA
[2] Institute for Materials Research, Tohoku University, Sendai 980-8577, Japan

E-mail: maria@anl.gov

Received 31 July 2009, in final form 8 October 2009
Published 3 December 2009
Online at stacks.iop.org/JPhysCM/22/015501

Abstract

We investigate the effect of individual atomic impurities on the superconducting state that they are embedded in. Using low temperature scanning tunneling microscopy and spectroscopy we could identify Co and Mn atoms in the Co_xNbSe_2 and Mn_xNbSe_2 single crystals and observe the influence on the local electronic density of states (LDOS) at 0.4 K. We find that Co is in the weak scattering limit. In this case the LDOS is quite homogeneous on the sample surface, despite the number of defects, and retains sharp coherent superconducting peaks. This is in strong contrast to the effects of Mn impurities, which locally destroy superconductivity. In this case the LDOS shows a strong enhancement of spectral weight inside the superconducting gap even far from the Mn atoms. Moreover, two impurity bound states are found within the superconducting gap at $E/\Delta_0 = 0.18$ and 0.36 at locations close to defects.

(Some figures in this article are in colour only in the electronic version)

1. Introduction

Magnetic impurities in s-wave superconductors break time-reversal symmetry and induce profound effects on the superconducting state such as lowering the superconducting critical temperature and giving rise to midgap states. The effect of an ensemble of magnetic impurities in a superconductor has been theoretically addressed by the pioneering work of Abrikosov and Gorkov [1] in the weak scattering Born limit approximation. In that work the authors predicted gapless superconductivity that was observed experimentally soon after [2]. The theory was extended to describe the effect of a single magnetic impurity by Yu, Shiba and Rusinov [3–5] that predicted the presence of bound states in the gap near the impurity atom. When increasing the concentration of magnetic impurities the interference between impurities should produce impurity bands starting from the bound state. Depending upon the strength of scattering the formation of Shiba bands will affect the density of states in a different way [6]. Experimental studies of magnetic impurities in superconductors have been focused mostly on bulk properties. The electronic density of states was measured using a planar tunnel junction with superconducting electrodes doped with magnetic impurities. The results show enhanced spectral weight in the gap region and subgap features [2, 7, 8]. More recently, the development of techniques that allow us to measure the local density of states (LDOS) near a single impurity stimulated extensive theoretical work [9–12]. The experiments using low temperature scanning tunneling spectroscopy allowed the observation of impurity states in high-T_c superconductors [13]. Although it may seem the subject has been widely studied, the only experimental works addressing the LDOS around a single impurity in an s-wave superconductor deal with magnetic adsorbates deposited on an Nb thin film surface [14] and recently on a Pb thin film [15]. The first one revealed the presence of quasiparticle excitations in the gap within few atomic distances from the impurity site. In [15] the midgap states are more clearly resolved by using a superconducting Nb tip.

[3] Present address: Institute of Electrical Engineering, Slovak Academy of Sciences, Dúbravská cesta 9, 84104 Bratislava, Slovakia.
[4] Present address: Center for Nanoscale Materials, Argonne National Laboratory, Argonne, IL 60439, USA.

In this paper we aim to bridge the gap between the pioneering work performed with planar tunnel junctions and the more recent STM work performed on magnetic atomic adsorbates on superconductors. Indeed, we measure LDOS by low temperature scanning tunneling spectroscopy in Co_xNbSe_2 and Mn_xNbSe_2 single crystals where the magnetic atoms (Co and Mn) are intercalated in the structure of the crystal and therefore they affect the bulk superconductivity as well. The choice of $NbSe_2$ as host material is based on the fact that it can be easily intercalated between the van der Waals coupled Se planes and can be easily cleaved, providing good surfaces for STM studies. We find a strikingly different effect on the tunneling spectra in Co_xNbSe_2 and Mn_xNbSe_2 single crystals. The tunneling spectra recorded far from impurities are very different in the two cases. In the case of Mn_xNbSe_2 the zero bias conductance increases much more rapidly than predicted by the Abrikosov–Gorkov theory. Moreover, close to impurities the shape of the spectra in the subgap region is also very different in the two cases. The tunneling spectrum strongly depends on location, it is asymmetric and tiny features are detected in the case of Mn impurities while in the case of Co the tunneling spectrum is much more homogeneous as a function of location without any feature in the gap.

2. Experiment

We investigate $NbSe_2$ single crystals with a dilute concentration of Co and Mn. Cobalt and manganese were intercalated in the $NbSe_2$ single crystals during growth in iodine vapor transport at 900 °C [16]. The x-ray diffraction pattern showed the same structure as 2H-$NbSe_2$.

The extended x-ray absorption fine-structure spectroscopy (EXAFS) experiment showed that no clustering of magnetic atoms is present in the range of concentrations studied. The Co and Mn content was determined by energy-dispersive x-ray microprobe analysis. The superconducting critical temperature was determined by superconducting quantum interference device (SQUID) magnetometry and measured in a small applied field ($H = 1$ Oe). In this paper we investigate samples with a dilute concentration of Co and Mn. The reduction in superconducting critical temperature T_c with increasing Co content is linear at a rate of about 3 K per at.% of Co and at about 25 K per at.% of Mn, in agreement with earlier reports [17–19]. Susceptibility measurements were performed on a Quantum Design MPMS system to investigate the magnetic state of Co and Mn in $NbSe_2$.

Low temperature scanning tunneling microscopy (STM) and spectroscopy (STS) have been performed at $T = (0.4 \pm 0.1)$ K using a Unisoku UHV ^{3}He STM system, with a base pressure of 1×10^{-10} Torr. Different surface treatments have been applied to prepare the samples for STM studies, including cleaving in He exchange gas and in UHV, and similar results have been observed. We used Pt–Ir tips in all of our experiments; therefore the tunneling conductance between a normal electrode (tip) and a superconducting sample directly provides the electronic density of states of the sample. Tunneling spectra have been acquired using the lock-in ac modulation technique while the I–V curve was acquired simultaneously to get the zero bias conductance value. Usually at least 20 curves were acquired at the same location and then averaged. The tunneling junction resistance was kept the same for all measurements reported in this paper and atomically flat surfaces were measured to minimize the variations in the tip–sample separation.

3. Results and discussion

Temperature dependence of the magnetic susceptibility, $\chi = M/H$, revealed the absence of magnetic ordering for both Co_xNbSe_2 and Mn_xNbSe_2 single crystals down to 1.8 K in the range of intercalation concentrations studied in this paper. Temperature dependence of the susceptibility χ follows a Curie–Weiss law [19]. From the fit of χ, in the range of temperatures below 100 K, we obtain an effective magnetic moment $\mu_{\rm eff} = 0.6\ \mu_B$ per Co atom in the case of $Co_{0.012}NbSe_2$ while for $Mn_{0.0012}NbSe_2$ we find $\mu_{\rm eff} = 4.2\ \mu_B$ per Mn atom. The small value of $\mu_{\rm eff}$ obtained in the case of Co is consistent only with $S = 1/2$, while in the case of Mn the value of $\mu_{\rm eff}$ is close to the spin-only moment of Mn^{3+}, with $S = 2$ consistent with data reported earlier in the literature [20]. The Curie–Weiss dependence of the susceptibility due to the presence of magnetic impurities suggests a coupling between the localized moments which is provided by the conduction-electron-mediated indirect exchange interaction of the Ruderman–Kittel–Kasuya–Yoshida (RKKY) type. This interaction decays with distance r as $J^2\frac{\cos(2k_Fr)}{r^3}$, where k_F is the Fermi momentum and J is the exchange potential. We obtain an estimate of the exchange potential J from the rate of suppression of the superconducting critical temperature with the concentration of magnetic impurities n [21, 22]:

$$\frac{dT_c}{dn} = -\frac{\pi^2}{8k_B}N(E_F)S(S+1)J^2, \qquad (1)$$

where $N(E_F)$ is the density of states at the Fermi level. Using the result that we obtained from the susceptibility data for the spin of Mn and Co and the value $N(E_F) = 1.73$ (eV molecule)$^{-1}$ from band structure calculations, we obtain $J = 0.13$ eV for Mn and $J = 0.12$ eV for Co. These estimates are in agreement with the estimates reported on Fe_xNbSe_2 [23] and they suggest that the magnitude of J is similar in both Mn_xNbSe_2 and Co_xNbSe_2.

Figure 1(a) shows a typical STM topography image obtained on a $Co_{0.012}NbSe_2$. The impurities show up as bright or dark spots. Similar images were obtained on freshly cleaved surfaces of Mn_xNbSe_2 crystals. We measured the tunneling density of states on a series of $NbSe_2$ crystals with and without magnetic impurities. Figure 1(b) shows three typical conductance spectra acquired at 0.4 K on $NbSe_2$, $Co_{0.012}NbSe_2$ and $Mn_{0.0012}NbSe_2$ single crystals far away from impurities. The Co- and Mn-doped $NbSe_2$ single crystals have superconducting critical temperatures of 5.7 K and 5.8 K, respectively. Despite the similar critical temperature the tunneling spectra are strikingly different. The spectrum on the Mn intercalated sample shows very broadened coherence peaks and a substantial increase of spectral weight within the superconducting gap while the spectrum of the Co_xNbSe_2

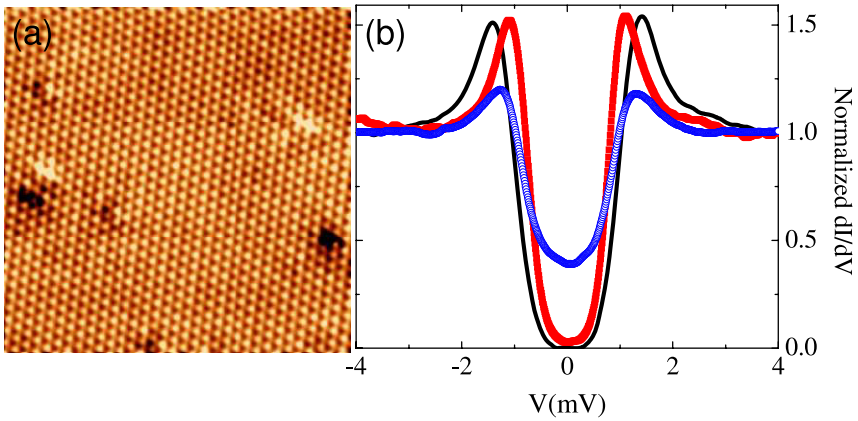

Figure 1. (a) Constant-current STM topography image acquired on a $Co_{0.012}NbSe_2$ single-crystal surface at a sample bias of $V = -100$ mV and tunneling current $I = 100$ pA. The scanning area is 10.5×10.5 nm^2. (b) Normalized tunneling conductance spectra in the case of pure $NbSe_2$ (solid line), $Co_{0.012}NbSe_2$ (full squares) and $Mn_{0.0012}NbSe_2$ single crystals (open circles). The spectra have been acquired far away from impurity atoms at $T = 0.4$ K with set point $V = -5$ mV and $I = 100$ pA.

crystal seems to be much less affected by the presence of Co atoms, despite the very different impurity concentration in the two cases. Indeed, it should be noted that the impurity concentration is 0.4 and 0.04 at.% in the case of Co_xNbSe_2 and Mn_xNbSe_2, respectively, which corresponds to about 70 impurities in a superconducting correlation volume in the case of the Co intercalated samples and less than 10 impurities in the case of Mn. In order to understand the striking difference between these spectra we consider the theoretical framework studied independently by Yu, Shiba and Rusinov [3–5] in the limit of classical spin. They found that the bound state energy is given by the expression:

$$\epsilon_0 = \frac{E_0}{\Delta_0} = \frac{1 - (JS\pi N(E_F))^2}{1 + (JS\pi N(E_F))^2}. \qquad (2)$$

In the case of weak scattering ($JSN(E_F) \ll 1$) the bound state will lie near the gap edge, while in the case of strong scattering ($JSN(E_F) \approx 1$) it will be deep in the gap. Interference between impurities will induce the formation of Shiba bands growing from the bound state and will affect the local density of states in a different way in the two cases. In the limit of weak scattering the results of Abrikosov–Gorkov theory [1] are recovered. On the other hand, in the limit of strong scattering the bound state is deep inside the gap and the impurity band grows starting from the Fermi energy towards the gap edge. Using equation (2) we estimate ϵ_0 for given J and S, and we obtain $\epsilon_0 = 0.33$ in the case of Mn_xNbSe_2 and $\epsilon_0 = 0.95$ in the case of Co_xNbSe_2. This analysis implies that there is a strong scattering from the Mn impurities and a weak scattering from the Co impurities, mainly due to a strong mixing of the d resonance with the conduction electrons.

In the vicinity of the Mn impurity the LDOS is also strongly modified. From topography images we could identify mainly three types of defects. The first type of defect consists of a region of approximately six atoms that looks brighter than the surrounding atoms (figure 2(a)). A typical tunneling spectrum recorded at this site is reported in figure 2(d). The coherence peaks are slightly suppressed and the zero bias conductance is enhanced compared to the spectrum recorded far away from the impurity site. The second type of defect is shown in figure 2(b) consisting of a bright spot always next to a darker spot. The spectra acquired at the bright and at the dark spot in this image are very similar (figure 2(e)). In this case both coherence peaks are suppressed. The third type of defect appears as a dark region (figure 2(c)). The spectra acquired close to the impurity site are very often asymmetric for extraction and injections of electrons. The conductance spectrum reported in figure 2(f) shows a stronger asymmetry. Indeed, the height of the coherence peaks for both polarities are asymmetric and there is an increase of spectral weight at positive bias that implies that it is easier to inject electrons at the impurity site. All these spectra are also V-shaped and reproducibly reveal small structures in the gap region. These small structures appear as kinks at energy positions symmetric with respect to E_F but their amplitudes are asymmetric as a result of the broken symmetry under the particle–hole transformation [14]. Different topographic and spectroscopic signature of defects can originate either from subsurface Mn defects or from the interference of impurities due to the presence of Mn dimers and trimers [15]. In figure 3(a) the evolution of the spectra is reported, starting from the impurity site shown in the inset and moving away from it. There are clear features in the gap when the spectrum is acquired at the location of the impurity. The states in the gap can be seen better by plotting the difference between the local density of states recorded at the impurity site and the one recorded far from it. In figure 3(b) the differences between the spectrum at that particular location and the one far from impurities are plotted, and the spectra are shifted vertically for clarity. There are clear peaks in the gap region that disappear quickly by moving away on a radius of about 3–4 atomic distances outside of the dark region. As shown in figure 3(b) these features are very tiny and they appear at energies $E_1 = \pm 0.2$ and $E_2 = \pm 0.4$ meV. The feature at $E_2 = \pm 0.4$ meV is in good agreement with the estimate for the bound state that we obtain from equation (2). The presence of additional structures can be explained by considering theories that include not only s-wave scattering of

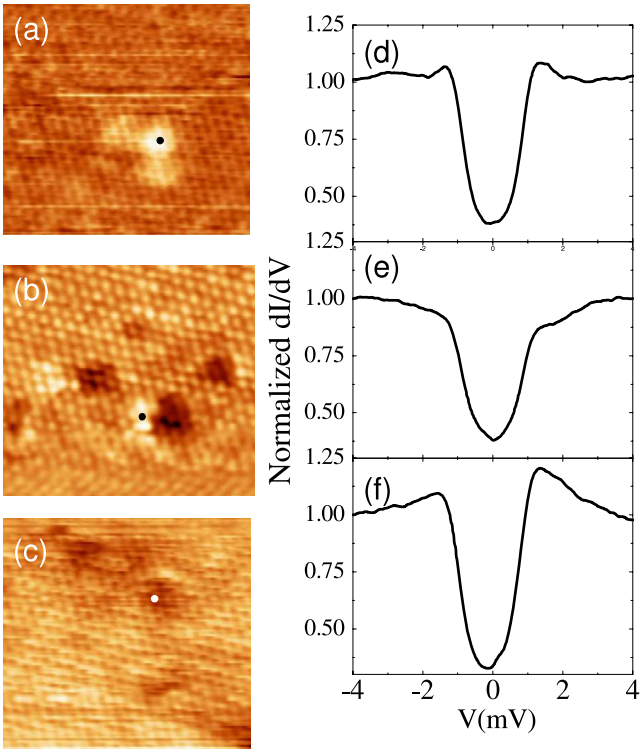

Figure 2. (a)–(c) Topography images of three typical defect patterns of near-surface Mn impurities in $Mn_{0.0012}NbSe_2$ (images were acquired in constant-current mode with $V = -100$ mV and $I = 100$ pA). The scanning area is 6.9×6.4 nm^2. (d) LDOS acquired at the impurity site shown with a dot in image (a). (e) LDOS acquired at the bright spot, shown with a dot, in (b). (f) LDOS acquired at the location shown with a dot in image (c). All the conductance spectra have been acquired with the same set point of $V = -5$ mV and $I = 100$ pA and normalized to the value of the conductance at -4 mV.

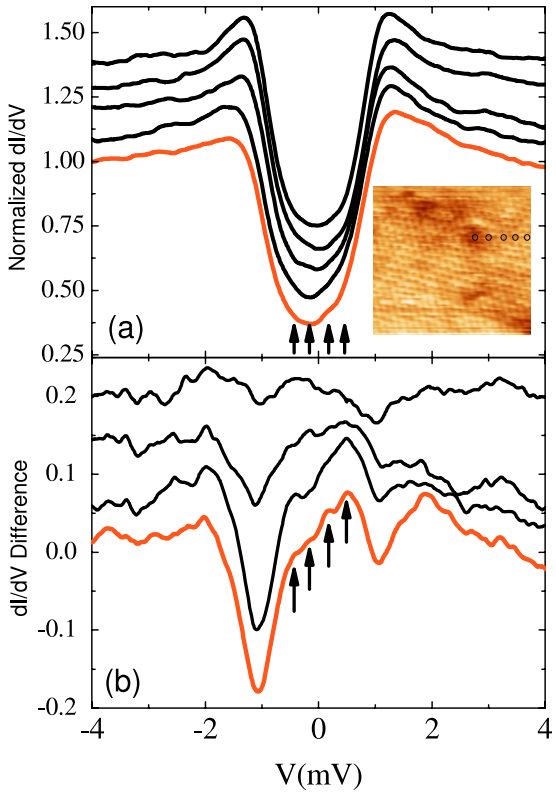

Figure 3. (a) Sequence of LDOS spectra acquired in the vicinity of an Mn atom. The inset shows local topography with the locations where the tunneling spectra have been acquired (circles). The spectra have been shifted for clarity (the bottom curve corresponds to the center of the dark spot shown in the inset). The scanning area is 6.9×6.4 nm^2 acquired at $V = -100$ mV and $I = 100$ pA. (b) The dI/dV difference between the curves in (a) and the reference spectrum acquired far from impurities. The arrows show the position of the peaks inside the energy gap at ± 0.2 and ± 0.4 mV. The background spectra used to obtain the difference spectra were taken at least 3.0 nm away from any impurity.

the conduction electrons from the magnetic impurity atoms, but also partial waves with higher orbital angular momentum ($l = 0, 1, 2 \ldots$) [24, 25]. According to [25] equation (2) of the suppression of T_c becomes

$$\frac{dT_c}{dn} = -\frac{1}{8k_B N(E_F)} \sum_l (2l+1)(1-\epsilon_l^2), \qquad (3)$$

where l is the orbital angular momentum and different bands ϵ_l are weighted by the factor $(2l + 1)$. By using the values of $\epsilon_{l=0} = 0.2$ meV$/\Delta_0 = 0.18$ and $\epsilon_{l=1} = 0.4$ meV$/\Delta_0 = 0.36$ we find that the suppression of T_c is $\approx$30 K/at.%, very close to the experimental value of 25 K/at.%.

Our results agree with earlier tunneling experiments performed on planar junctions of Pb–Mn systems, in showing that the energy gap is more rapidly filled with states than predicted by the Abrikosov–Gorkov theory. Two impurity bands could be resolved in SIN planar junctions for small concentrations of magnetic impurities (<780 ppm of Mn in Pb–Mn alloy [7]) as well as in SIS junctions [8]. However, when the magnetic impurity concentration was larger (0.13 at.% [2]) no well-defined impurity band was detected and the tunneling data showed only an enhanced density of states inside the gap. Therefore, we believe that the subgap features that we detect in the Mn_xNbSe_2 crystals close to impurities are small due to interference between impurities and they could be better resolved for lower concentrations of Mn.

The situation is quite different in the case of Co_xNbSe_2. The LDOS is much more homogeneous as a function of the position on the sample surface although the STM topography images show the presence of many defects. In most of the cases at the defect site we mostly observe only minute differences in the LDOS, like small suppression of peak height or very small changes in peak position. In figure 4 the solid line is a dI/dV spectrum measured far from defects showing very pronounced coherence peaks at 1.1 meV. It should be noted at this point that even a tunneling spectrum of pure $NbSe_2$ cannot be simply reproduced by a single-gap s-wave DOS [26]. Indeed, two-gap superconductivity in $NbSe_2$ was suggested from angle-resolved photoemission spectroscopy [27] and more recently from specific heat [28] and London penetration depth measurements [29]. In tunneling spectra at 100 mK the smaller gap can be seen as a kink at about 0.5 mV [30]. When the temperature is increased this kink is washed out but the tunneling spectra show coherent peaks that

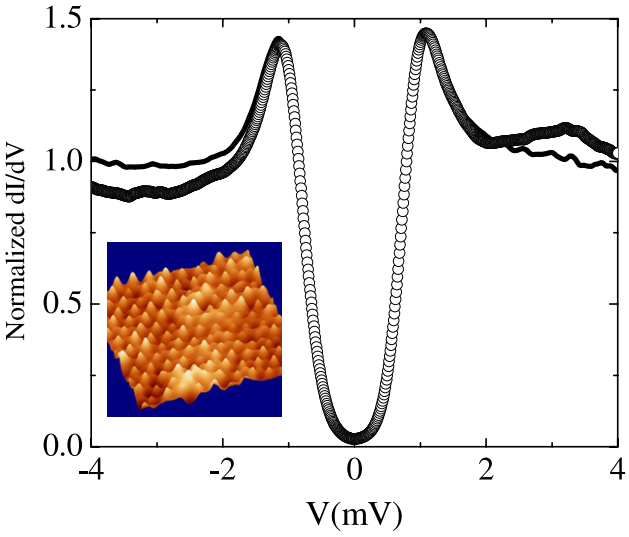

Figure 4. LDOS acquired on a $Co_{0.012}NbSe_2$ crystal away from impurity (solid line) and at the impurity site (open circles). The inset shows an STM topography zooming in on a region with defects. The scanning area is 4.2×4.2 nm^2.

are smaller than the BCS prediction. In our data in the case of Co_xNbSe_2, the shift at lower energy of the coherence peak by about 20%, compared to pure $NbSe_2$, is consistent with a suppressed critical temperature of about the same amount (from 7.15 to 5.7 K). Occasionally, for a small fraction of defects we observe an asymmetric conductance curve at the impurity site that reveals a broad peak for $eV > \Delta$. However, no peaks are ever observed within the gap region, as shown in figure 4. These asymmetric spectra, when observed, are very local and quickly disappear on a few atomic distances from the defect location. Asymmetric STM tunneling spectra have been reported in the case of Co atoms adsorbed on Au(111) surfaces [31]. This asymmetric dI/dV lineshape that becomes symmetric when the STM tip moves outward from the Co atom has been identified as Kondo resonance. Since the effective magnetic moment measured for the Co_xNbSe_2 samples reported here is quite small ($\mu_{\rm eff} = 0.6\ \mu_{\rm B}$), the main question to address is whether Kondo physics is playing any role in this case. The susceptibility data show a Curie–Weiss behavior [19]: therefore if there is any screening of the Co magnetic moment it can be only partial. Resistivity measurements down to 1.8 K do not show any evidence of a Kondo temperature [32]. Therefore, we do believe that the presence of a Kondo effect in the case of Co_xNbSe_2 is still controversial and requires further investigations.

4. Summary

In conclusion, we have presented STM and STS data on Co_xNbSe_2 and Mn_xNbSe_2 single crystals at 0.4 K. The main difference between the two cases is that Co is in the low spin configuration ($S = 1/2$) and Mn is in the high spin configuration ($S = 2$), as determined from susceptibility measurements. Tunneling spectroscopy reveals that Mn atoms act as strong scatterers by destroying superconductivity locally while Co atoms do not. Close to Mn atoms the LDOS also reveals subgap structures that disappear quickly by moving 3–4 atoms away from the defect site. These subgap structures have not been observed in the case of Co_xNbSe_2. Co atoms act as a weak scatterer, due to a strong hybridization with the conduction electrons. As a consequence, the LDOS is much more homogeneous as a function of location on the sample surface and have less states in the gap.

Acknowledgments

The authors would like to thank K Matveev, A Koshelev and A Balatski for useful discussions. We also would like to acknowledge the support by the International Frontier Center for Advanced Materials (IFCAM) at Tohoku University, Japan (MI). This work as well as the use of the Center for Nanoscale Materials and the Electron Microscopy Center at Argonne National Laboratory was supported by UChicago Argonne, LLC, Operator of Argonne National Laboratory ('Argonne'). Argonne, a US Department of Energy Office of Science laboratory, is operated under contract no. DE-AC02-06CH11357.

References

[1] Abrikosov A A and Gor'kov L P 1960 *Zh. Eksp. Teor. Fiz.* **39** 1781
Abrikosov A A and Gor'kov L P 1961 *JETP* **12** 1243 (Engl. Transl.)
[2] Woolf M A and Reif F 1965 *Phys. Rev.* **137** A557
[3] Yu L 1965 *Acta Phys. Sin.* **21** 75
[4] Shiba H 1968 *Prog. Theor. Phys.* **40** 435
[5] Rusinov A I 1968 *Zh. Eksp.Teor. Fiz. Pis'ma Red.* **9** 146
Rusinov A I 1969 *JETP* **9** 85 (Engl. Transl.)
[6] Balatsky A V, Vekhter I and Zhu J-X 2006 *Rev. Mod. Phys.* **78** 373 and references therein
[7] Bauriedl W, Ziemann P and Buckel W 1981 *Phys. Rev. Lett.* **47** 1163
[8] Tsang J K and Ginsberg D M 1980 *Phys. Rev.* B **21** 132
[9] Flatte M E and Byers J M 1997 *Phys. Rev. Lett.* **78** 3761
[10] Salkola M I, Balatski A V and Shriffer J R 1997 *Phys. Rev.* B **55** 12648
[11] Flatte M E and Byers J M 1997 *Phys. Rev.* B **56** 11213
[12] Flatte M E and Reynolds D E 2000 *Phys. Rev.* B **61** 14810
[13] Hudson E W, Lang K M, Madhavan V, Pan S H, Eisaki H, Uchida S and Davis J C 2001 *Nature* **411** 920
[14] Yazdani A, Jones B A, Lutz C P, Crommie M F and Eigler D M 1997 *Science* **275** 1767
[15] Ji S H, Zhang T, Fu Y S, Chen X, Ma X C, Li J, Duan W H, Jia J F and Xue Q K 2008 *Phys. Rev. Lett.* **100** 226801
[16] Oglesby C S, Bucher E, Kloc C and Hohl H 1994 *J. Cryst. Growth* **137** 289
[17] Hauser J J, Robbins M and DiSalvo F J 1973 *Phys. Rev.* B **8** 1038
[18] Gras J P, Haen P, Monceau P, Waysand G, Molinie P and Rouxel J 1977 *Nuovo Cimento* B **38** 519
[19] Iavarone M, Di Capua R, Karapetrov G, Koshelev A E, Claus H, Rosenmann D, Malliakas C, Kanatzidis M, Nishizaki T and Kobayashi N 2008 *Phys. Rev.* B **78** 174518
[20] Voorhoeve-van Den Berg J M and Sherwood R C 1970 *J. Chem. Solids* **32** 167
[21] Caroli B 1975 *J. Phys. F: Met. Phys.* **5** 1399
[22] Skalski S, Betbeder-Matibet O and Weiss P R 1964 *Phys. Rev.* A **136** 1500

[23] Whitney D A, Fleming R M and Coleman R V 1977 *Phys. Rev.* B **15** 3405
[24] Rusinov A I 1969 *Zh. Eksp. Teor. Fiz.* **56** 2047
Rusinov A I 1969 *Sov. Phys.—JETP* **29** 1101 (Engl. Transl.)
[25] Kunz A B and Ginsberg D M 1980 *Phys. Rev.* B **22** 3165
[26] Rodrigo J G and Viera S 2004 *Physica* C **404** 306
[27] Yokoya T, Kiss T, Chainani A, Shin S, Nohara M and Takagi H 2001 *Science* **294** 2518
[28] Huang C L, Lin J-Y, Chang Y T, Sun C P, Shen H Y, Chou C C, Berger H, Lee T K and Yang H D 2007 *Phys. Rev.* B **76** 212504
[29] Fletcher J D, Carrington A, Diener P, Rodière P, Brison J P, Prozorov R, Olheiser T and Giannetta R W 2007 *Phys. Rev. Lett.* **98** 057003
[30] Guillamon I, Suderow H, Guinea F and Vieira S 2008 *Phys. Rev.* B **77** 134505
[31] Madhavan V, Chen W, Jamneala T, Crommie M F and Wingreen N S 1998 *Science* **280** 567
[32] Iavarone M, Karapetrov G, Di Capua R, Koshelev A E, Rosenmann D, Claus H, Kwok W K, Nishizaki T and Kobayashi N 2009 *J. Phys.: Conf. Ser.* **150** 052073